Applied Catalysis B: Environmental 264 (2020) 11855 3

Contents lists available at ScienceDirect

Applied Catalysis B: Environmental

journal homepage: www.elsevier.com/locate/apcatb

Self-limiting growth of ligand-free ultrasmall bimetallic nanoparticles on carbon through under temperature reduction for highly efficient methanol electrooxidation and selective hydrogenation

Mingzhen Hu[a,b], Lei Jin[b], Yuanyuan Zhu[c,d], Lei Zhang[a,b], Xingxu Lu[d], Peter Kerns[b], Xingsong Su[a,b], Sen Cao[b], Puxian Gao[c,d], Steven L. Suib[b,c,d], Ben Liu[a,*], Jie He[b,c,**]

[a] Jiangsu Key Laboratory of New Power Batteries, Collaborative Innovation Center of Biomedical Functional Materials, School of Chemistry and Materials Science, Nanjing Normal University, Nanjing 210023, China [b] Department of Chemistry, University of Connecticut, Storrs, CT 06269, United States [c] Institute of Materials Science, University of Connecticut, Storrs, CT 06269, United States

[d] Department of Materials Science and Engineering, University of Connecticut, Storrs, CT 06269, United States

ARTICLEINFO

Keywords:
Self-limiting growth
Ultrasmall bimetallics
Ligand-free nanoparticles
Under temperature reduction
Methanol electrooxidation
Hydrogenation

ABSTRACT

We report a self-limiting growth method of ultrasmall Pd-containing bimetallic nanocatalysts supported on carbon through under temperature reduction (UTR). The UTR phenomenon is observed for the (co)reduction of a second base metal precursor (M = Co, Ni, and Zn) below its thermodynamic reduction temperature in the presence of Pd. The origin of the UTR phenomenon lies in the hydrogen spillover of Pd to drive the (co)reduction of the base metal at the temperature below its thermodynamic reduction temperature; while, the further reduction is shut down simultaneously to limit the overgrowth of nanoparticles when forming nanoalloys. Using nitrided carbon as a support, we demonstrate the self-limiting growth of three Pd-containing nanoalloys, including $Pd_{1.7}Co$, $Pd_{1.6}Ni$ and Pd_2Zn, with average sizes around 1.5 nm using UTR. Sub-2 nm Pd-containing bimetallic nanoalloys exhibited excellent catalytic properties in both methanol electrooxidation and selective hydrogenation of cinnamaldehyde.

1. Introduction

Supported precious metal nanocatalysts on carbon are of great importance in various chemical transformations. When adding a second inexpensive base metal (e.g., M = Co, Ni, and Zn) to form nanoalloys, the decrease in the content of noble metals not only reduces cost and but brings interesting catalytic synergies. For example, nanoalloys consisting of base and noble metals show interesting interfacial effects, including electronic and geometrical advantages, that improve catalytic performance of bimetallic nanocatalysts significantly [1,1–7]. The most common method to synthesize supported bimetallic nanoalloys is impregnation and co-reduction of two metal precursors on substrates [8,9]. While there are a number of nanoalloys (e.g., Pd-containing nanoparticles, NPs) that show improved catalytic activities compared to pure Pd [10], the co-reduction yields bimetallic NPs in a broad size distribution and nonuniform alloying [11].

In terms of the high atom efficiency as catalysts, ultrasmall nanoalloys (< 2 nm) are highly desirable [12,1–15]. The synthesis of such nanoalloys on carbon is technically challenging given the large surface energy favoring to aggregate [16]. To grow bimetallic nanoalloys of noble and base metal pairs on carbon, co-impregnation of two metal precursors did not provide satisfactory alloying neither in terms of the composition and size of nanoalloys [17,18]. The main synthetic challenges are two-fold: i) competitive adsorption on carbon which limits the content of base metals; and ii) differences in redox potential of noble and base metal pairs making it challenging to reduce them concurrently to form alloys.

We report a simple self-limiting growth method to directly grow ultrasmall bimetallic nanoalloys of noble (Pd-based as examples) and base metal pairs on nitrided Printex U carbon (NC). The method is based on the co-impregnation of two metal precursors where metal cations are co-adsorbed through the metal-N coordination. Since the NC

* Corresponding author at: Jiangsu Key Laboratory of New Power Batteries, Collaborative Innovation Center of Biomedical Functional Materials, School of Chemistry and Materials Science, Nanjing Normal University, Nanjing 210023, China.

** Corresponding author at: Department of Chemistry, University of Connecticut, Storrs, CT 06269, United States. E-mail addresses: ben.liu@njnu.edu.cn, liuben3084@gmail.com (B. Liu), jie.he@uconn.edu (J. He).

https://doi.org/10.1016/j.apcatb.2019.118553

Received 27 September 2019; Received in revised form 11 December 2019; Accepted 19 December 2019 Available online 20 December 2019

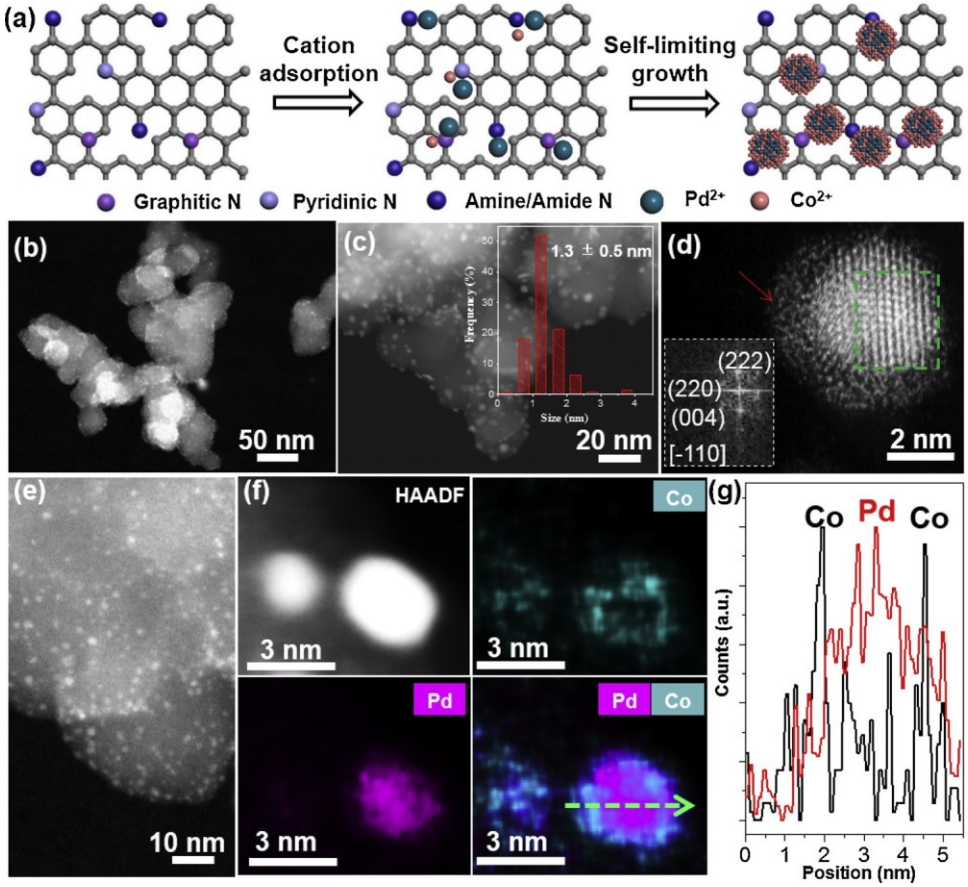

Fig. 1. (a) Scheme of the self-limiting growth of bimetallic nanoalloys. (b,c) HAADF-STEM, (d,e) aberration-corrected STEM, (f) EDS mapping and (g) corresponding EDS line profile of $Pd_{1.7}Co$.

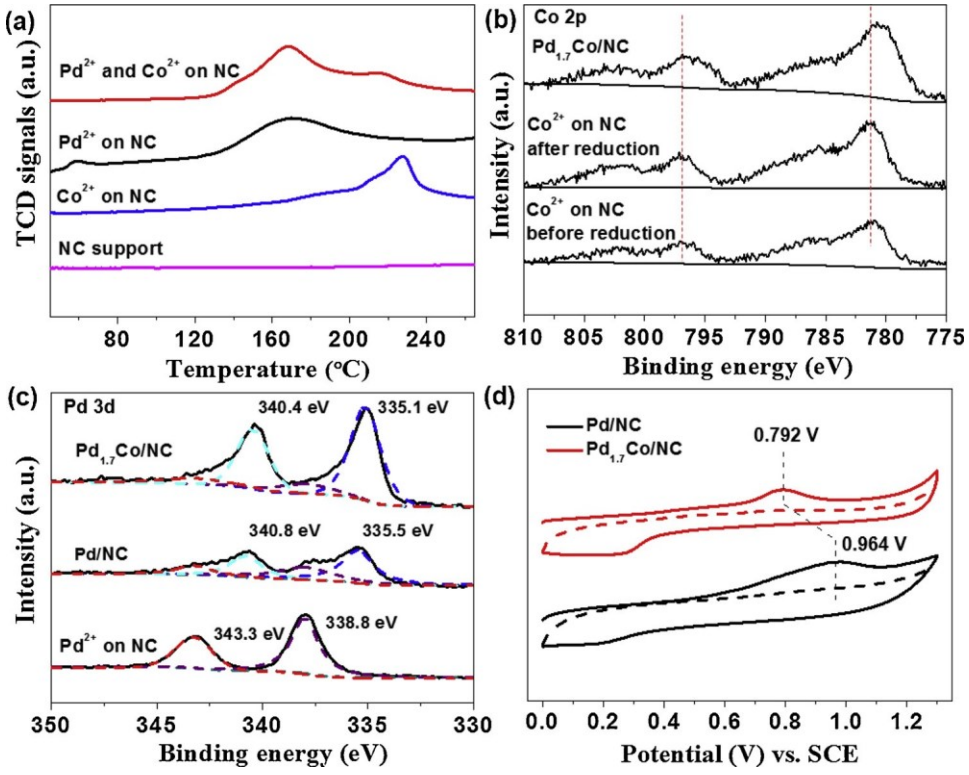

Fig. 2. (a) H_2-TPR of pure Pd^{2+} and Co^{2+} on NC. (b) High-resolution Co 2p and (c) Pd 3d XPS spectra of $Pd_{1.7}Co$, precursors before reduction. (d) CO striping voltammograms of $Pd_{1.7}Co$ and Pd.

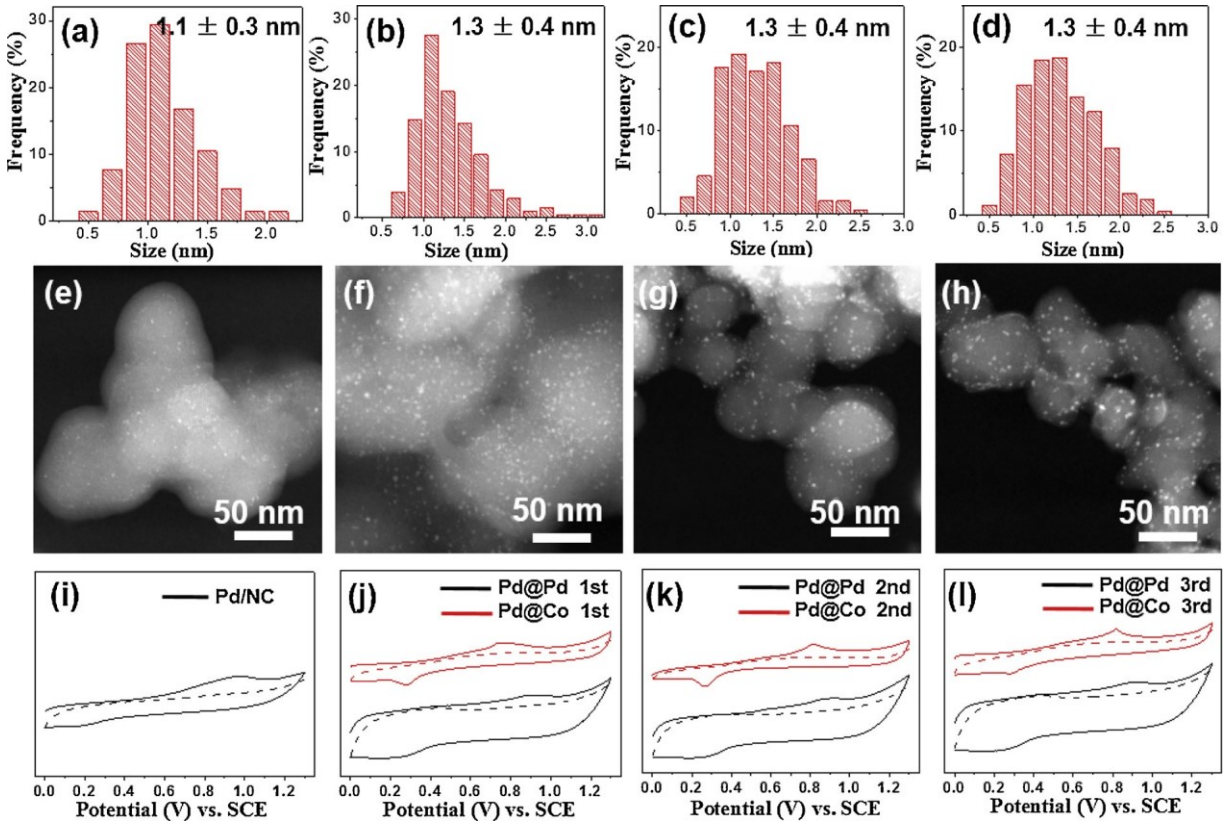

Fig. 3. (a–d) Size distribution histograms, (e–h) HAADF-STEM images, and (i–l) CO striping voltammetry of Pd (~1.1 nm) on NC and three continuous Co coating on Pd.

is highly selective to adsorb noble metal ions (Fig. S1), co-impregnation of the two metal ions was carried out at extremely high ratio with much excess base metals. To avoid consecutive heterogeneous nucleation of the two metals, for the first time, we demonstrate the under temperature reduction (UTR) for the synthesis of Pd-containing bimetallic nanoalloys below its thermodynamic reduction temperature, similar to underpotential deposition [19]. The UTR shows excellent control of nanoalloy size, because of the self-limiting process by hydrogen spillover on nanoalloys. Three Pd-containing ligand-free sub-2 nm nanoalloys, including $Pd_{1.7}Co$, $Pd_{1.6}Ni$ and Pd_2Zn (Pd_xM, x represents the ratio of Pd to M), were prepared through UTR. This conceptually new and cost-effective self-limiting growth strategy will largely simplify the preparation of ultrasmall nanoalloys.

2. Results and discussion

The synthesis of Pd-based bimetallic nanoalloys was carried out through co-impregnation route. NC (ca. 50 nm in diameter, nitrided Printex U carbon) was prepared through soft nitriding as reported previously (Fig. S2) [20,1–22]. For $Pd_{1.7}Co$, the co-impregnation of Na_2PdCl_4 and $Co(NO_3)_2$ was examined batchwise at various Pd-to-Co ratios. There is a remarkable difference in the binding/adsorption capability of the two metals on NC (Fig. S1) [23,24]. For the Pd-to-Co mole ratio ranging from 0.02 to 0.005, ~100 times adsorption selectivity for Na_2PdCl_4 is seen compared to $Co(NO_3)_2$. The interaction of anionic $PdCl_4^{2-}$ with NC is likely due to the enhanced adsorption through electrostatic attraction [25,26]. At a Pd-to-Co ratio of 0.01 in solution, the adsorbed Pd-to-Co ratio was measured to be 1.7 ± 0.3. In preparation, Co contents are identified in the washing solution (Fig. S3), due to the great adsorption difference between Pd and Co.

$Pd_{1.7}Co$ nanoalloys were produced by reduction of Pd and Co coimpregnated NC with hydrogen (H_2) at 200 °C ($Pd_{1.7}Co$/NC, see Supplementary Material (SM) for details). Scanning transmission electron microscopy (STEM, Fig. 1b–c) confirms the uniform size of $Pd_{1.7}Co$ nanoalloys. The diameter of $Pd_{1.7}Co$ is 1.3 ± 0.5 nm (Fig. 1c). Aberration-corrected STEM images in Fig. 1d-e reveal that most of nanoalloys are amorphous (see Fig. S4 for more images). Meanwhile, large NPs with a diameter > 2 nm show a core-shell nanostructure with a crystalline core as revealed in Fig. 1d. The fast Fourier transform (FFT) pattern along the [−110] axis (the inset of Fig. 1d) confirms that these lattice fringes are assigned to (222), (220) and (004) planes of slightly distorted face-centered cubic Pd. The outer shell with a lower brightness is assigned to a Co-rich alloyed phase in comparison with the bright core due to the difference in electron density. The loading amount of Pd is measured to be 1.1 wt% with a Pd-to-Co ratio of 1.7:1 (mol) using inductively coupled plasma mass spectrometry (ICP-MS).

Bimetallic compositions of $Pd_{1.7}Co$ nanoalloys were studied using energy dispersive X-ray spectroscopy (EDS) (Fig. 1f). The mapping confirms the co-existence of Pd and Co. The small particle is randomly alloyed. No core-shell structure is observed for sub-2 nm $Pd_{1.7}Co$ nanoparticles as shown in Fig. 1f. The larger particle is core-shell, again, with a Pd-rich core and Co-rich shell similar to that from high-resolution STEM observations (Fig. 1d). This is also seen in the line scan profile of Pd and Co distribution in Fig. 1g.

The bulk amorphous nature of $Pd_{1.7}Co$ was confirmed by X-ray diffraction (XRD). A very broad diffraction peak is seen for $Pd_{1.7}Co$ (Fig. S5). As controls, the co-impregnation on unmodified carbon led to the formation of larger NPs with mixed phases (Pd, Co and PdCo alloys, see TEM and XRD in Fig. S6). This indicates the role of surface nitrogen sites in stabilizing the initial nucleus and avoiding the overgrowth of single metal phases [22].

To gain insight into the formation mechanism of nanoalloys, temperature-programmed reduction with hydrogen (H_2-TPR) analysis was used to examine the reduction temperature of the two metal precursors (Fig. 2a). Na_2PdCl_4 on

NC displayed a reduction peak at ca. 170 °C, consistent with the reported value [27]. As for $Co(NO_3)_2$, the reduction

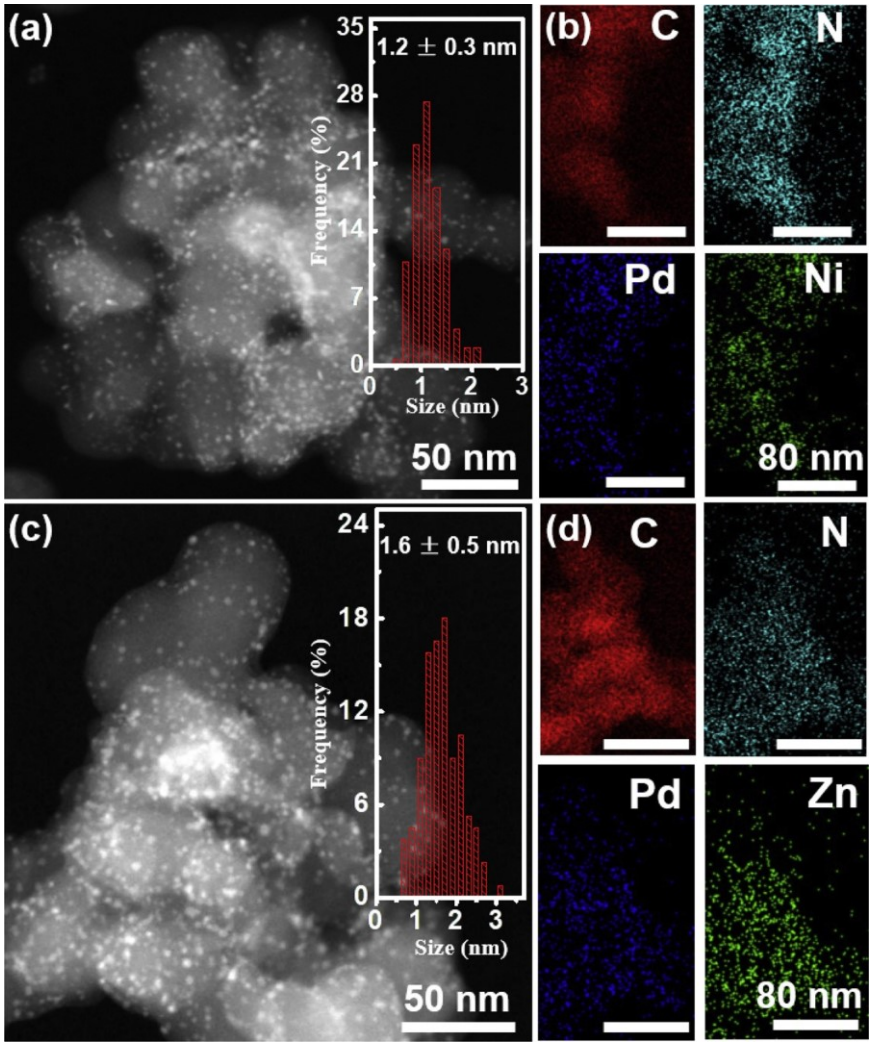

Fig. 4. (a) STEM image and (b) corresponding EDS mapping image of the sub-2 nm $Pd_{1.6}Ni$ nanoalloys supported on NC. (c) STEM image and (d) corresponding EDS mapping image of the sub-2 nm Pd_2Zn nanoalloys supported on NC. The insets of (a) and (c) are the particle-size distribution histograms of the $Pd_{1.6}Ni$ and Pd_2Zn nanoalloys.

peak was found at ca. 230 °C; while, the co-reduction of $Co(NO_3)_2$ with Na_2PdCl_4 resulted in an obvious shift towards a lower temperature of 210 °C. $Co(NO_3)_2$ solely was not reduced at 200 °C, as revealed by TEM and EDS mapping (Figure S7). Co 2p X-ray photoelectron spectroscopy (XPS) in Fig. 2b shows the unchanged binding energy as $Co(NO_3)_2$ after reduction at 200 °C. Whereas, in the absence of $Co(NO_3)_2$, ultrasmall Pd NPs (~1.1 nm Figs. 3e and Fig. S8) can be produced. Those results suggest that Pd drives the synergistic catalytic co-reduction of Co. Since Pd shows a much lower hydrogen dissociation energy [28], the hydrogen spillover effect from Pd to Co likely promotes the (co)reduction of $Co(NO_3)_2$ to drive the formation of Pd-Co nanoalloys below its thermodynamic reduction temperature.

To confirm the UTR of Co, XPS and carbon monoxide (CO) stripping voltammetry are used to reveal the electronic states of Pd and Co in $Pd_{1.7}Co$ nanoalloys. First, for Co 2p (Fig. 2b), the Co $2p_{3/2}$ and $2p_{1/2}$ peaks appear at 780.8 and 796.4 eV, which agrees with the reported values in PdCo NPs [29,30]. For Pd 3d (Fig. 2c), two asymmetric peaks at 335.1 and 340.4 eV are seen for Pd $3d_{5/2}$ and $3d_{3/2}$, respectively. The binding energy is close to that of metallic Pd [31]. By comparison, the Pd 3d peaks of pure Pd on NC are observed at 335.5 and 340.8 eV, showing a 0.4 eV positive shift as compared with $Pd_{1.7}Co$. This indicates that Co displays electron back-donation to Pd. This lowers the binding energy of Pd 3d [32], which is indicative of the formation of Pd-Co alloys. Second, we used CO stripping voltammetry to examine the change in surface properties of Pd. The stripping potential of $Pd_{1.7}Co$ (0.792 V vs. saturated calomel electrode (SCE), same hereafter) shows a 172 mV negative shift relative to pure Pd (0.964 V) (Fig. 2d). This is indicative of the formation of a bimetallic surface that weakens CO adsorption and lowers the oxidation potential of CO [33].

A series of control experiments were carried out to confirm the UTR of $Co(NO_3)_2$. Using Pd (~1.1 nm Fig. 3a) supported on NC as seeds, Co $(NO_3)_2$ was adsorbed in another impregnation process. After reduction at 200 °C, the average size of Pd-Co increased slightly to 1.3 nm (Fig. 3b). The CO stripping potential of the Pd-Co exhibits a 157 mV negative shift in comparison with that of initial Pd NPs (Fig. 3j). This closely agrees with that of $Pd_{1.7}Co$. The formed Pd-Co alloy is driven by the hydrogen spillover effect of Pd seeds to reduce $Co(NO_3)_2$ [34]. In addition, when repeating the Co impregnation and reduction for two more times (Fig. 3g–h), the average sizes of Pd-Co remain as 1.3 nm. In the meantime, similar CO stripping potentials (0.811 and 0.791 V) were observed for the further impregnation (Fig. 3k–i). Those results suggest that the formation of Pd-Co alloys on the initial Pd seeds prevented further reduction of $Co(NO_3)_2$ thus limiting overgrowth of Pd-Co alloys. The broad XRD peaks of these Co-coated Pd NPs in Figure S9 confirm the small size of nanoalloys. This self-limiting is possible because the reduction of $Co(NO_3)_2$ was carried out under its thermodynamic reduction temperature. By comparison, the consecutive Pd growth on Pd NPs led to a much broad size distribution while retaining similar CO

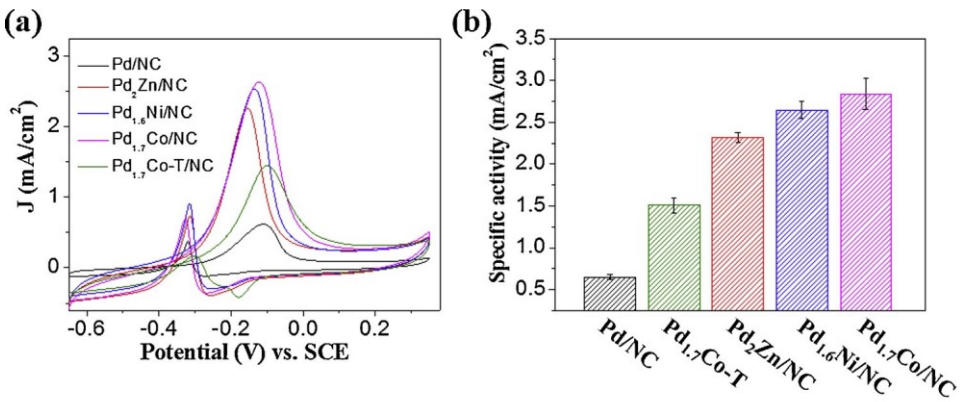

Fig. 5. (a) MOR CV curves measured in 0.1 M KOH with 1 M methanol and (b) specific activities of $Pd_{1.7}Co/NC$, $Pd_{1.6}Ni/NC$, Pd_2Zn/NC, $Pd_{1.7}Co$-T/NC and Pd/NC. The values in (b) were averaged from three independent measurements. (c) Chronoamperometry curves of $Pd_{1.7}Co/NC$ and Pd/NC at -0.1 V (SCE) in 0.1 M KOH with 1 M methanol. (b) Current density loss percent over $Pd_{1.7}Co/NC$ and Pd/NC as a function of time as derived from (c).

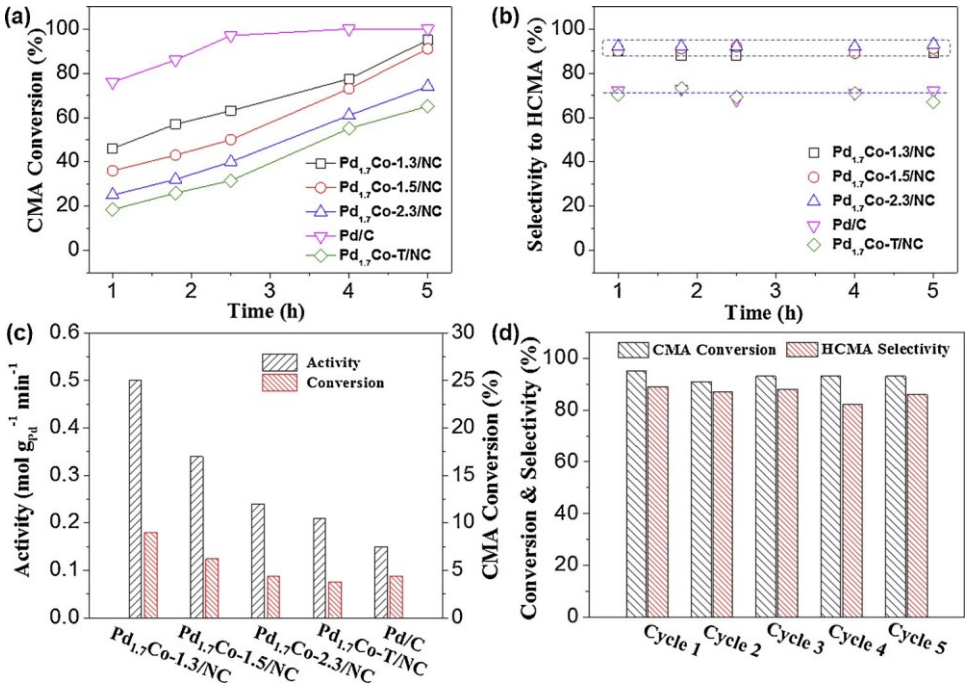

Fig. 6. (a) Cinnamaldehyde (CMA) conversion and (b) hydrocinnamaldehyde (HCMA) selectivity as a function of time over the 1.3 ±0.5 nm $Pd_{1.7}Co$ nanoalloys on NC ($Pd_{1.7}Co$-1.3/NC), 1.5 ± 0.5 nm on NC ($Pd_{1.7}Co$-1.5/NC) and 2.3± 0.7 nm $Pd_{1.7}Co$ on NC ($Pd_{1.7}Co$-2.3/NC), Pd-Co nanpparticles on NC obtained by thermodynamic growth ($Pd_{1.7}Co$-T/NC), and commercial Pd/C catalysts. (c) The specific rates of the prepared $Pd_{1.7}Co$-1.3/NC, $Pd_{1.7}Co$-1.5/NC, $Pd_{1.7}Co$-2.3/ NC, $Pd_{1.7}Co$-T/NC and commercial Pd/C catalysts. (d) Recycle experiment of the 1.3 ± 0.5 nm $Pd_{1.7}Co$ nanoalloys. The selective hydrogenation of cinnamaldehyde kinetics testing was carried out at 50 °C and 50 psi (pounds per square inch) under varied reaction times. The catalytic stability measurements are conducted at 50 °C and 50 psi for 5 h.

stripping potentials (Fig. 3j–l for CO stripping and Figure S10 for TEM).

When reducing above the thermodynamic reduction temperature of $Co(NO_3)_2$, e.g., 400 °C, larger NPs (~4.2 nm) were obtained (denoted as $Pd_{1.7}Co$-T/NC, same hereafter) as shown in Figure S11. The phase separated Pd and Co phases were seen from XRD (Figure S12a) and EDS elementary mappings (Fig. S13). By comparison, when annealing $Pd_{1.7}Co/NC$ under nitrogen at 400 °C even for 12 h, no phase separation peaks of Pd or Co were observed from XRD (Fig. S12b). This result further reveals the key importance of UTR in avoiding heterogeneous nucleation of Co.

The self-limiting growth is applicable to other systems, e.g., $Pd_{1.6}Ni$ and Pd_2Zn. As-synthesized $Pd_{1.6}Ni$ and Pd_2Zn are homogeneously dispersed on NC (defined as $Pd_{1.6}Ni/NC$ and Pd_2Zn/NC). The average particle sizes for $Pd_{1.6}Ni$ and Pd_2Zn are 1.2 ± 0.3 nm and 1.6 ± 0.5 nm, respectively as displayed in Fig. 4. The alloy nature of $Pd_{1.6}Ni$ and Pd_2Zn is confirmed by CO stripping voltammetry (Figures S14-S15), where a negative shift of 132 mV and 114 mV in the stripping potential was observed, respectively, in comparison with Pd.

Electrocatalytic methanol oxidation reaction (MOR) was first used to evaluate catalytic properties of these nanoalloys. The typical cyclic voltammograms (CVs) are given in Fig. 5. First of all, nanoalloys show a lower oxidation peak potential and higher peak current density in comparison with those of pure Pd. $Pd_{1.7}Co/NC$ shows a peak current density of 2.8 ± 0.2 mA cm^{-2} at −0.12 V, while the peak current densities of pure Pd/NC and $Pd_{1.7}Co$-T/NC are measured to be 0.7 ±0.1 mA cm^{-2} and 1.5 ± 0.1 mA cm^{-2} at −0.10 V.

The peak current density normalized to electrochemical active surface area (ECSA, Figure S16), or specific activity, is a reflection of intrinsic activity for electrocatalysts [35,36]. The specific activity of $Pd_{1.7}Co$/NC is approximately 4 times better than pure Pd and 2 times better than $Pd_{1.7}Co$-T/NC. The increase in intrinsic activity is attributed to the formation of alloys that varied the surface electronic state of Pd [37,37–39]. Similarly, mass activities of nanoalloys are higher than that of pure Pd (Fig. S17). The current intensity ratio of J_f (in the forward scan) to J_b (in the backward scan) is related to surface poisoning, that is the accumulation of carbonaceous residues during the forward cycle of the cyclic voltammetry. A higher J_f/J_b indicates smaller accumulation on a more active electrochemical surface. As plotted in Figure S18, the J_f/J_b values of $Pd_{1.7}Co$/NC is 3.57, far better than that of Pd/NC (1.62), indicating more active electrochemical surface and better anti-poisoning ability of $Pd_{1.7}Co$/NC. The catalytic stability is of great importance for fuel cell applications [40]. We carried out electrocatalytic stability tests of $Pd_{1.7}Co$/NC and Pd/NC using chronoamperometry (i-t curves). As shown in Fig. 5c–d, the $Pd_{1.7}Co$/NC displays much better electrocatalytic stability than Pd/NC at -0.1 V. The current density of the $Pd_{1.7}Co$/NC retains about 40% after 1800s testing, which is quite similar to previous reports [41,1–45]. By contrast, the Pd/NC displays a sharp drop of current density close to 0 mA/cm^2 within 1500s.

The ultrasmall size, monodispersity and clean surface also impart these sub-2 nm Pd-based nanoalloys with great potentials for heterogeneous catalysis applications. We further take the 1.3 ± 0.5 nm $Pd_{1.7}Co$/NC as an example for selective hydrogenation of cinnamaldehyde (CMA) evaluations. 1.5 ± 0.5 nm $Pd_{1.7}Co$/NC and 2.3 ±0.7 nm $Pd_{1.7}Co$/NC nanoparticles were prepared as control catalysts (see SM for details, Figure S19). As shown in Fig. 6a and b, the $Pd_{1.7}Co$/NC nanoparticles demonstrated excellent catalytic activity and selectivity in the testing time range. The catalytic activity of 1.3 ± 0.5 nm $Pd_{1.7}Co$/NC is much higher than that of 1.5 ±0.5 nm and 2.3 ± 0.7 nm $Pd_{1.7}Co$/NC nanoparticles coupled with excellent hydrocinnamaldehyde (HCMA) selectivity (around 90%). As displayed in Fig. 6c, the specific rates of the 1.3 ± 0.5 nm, 1.5 ±0.5 nm and 2.3 ±0.7 nm $Pd_{1.7}Co$/NC nanoparticles are calculated to be 0.5 mol_{CMA} min^{-1} g_{Pd}^{-1}, 0.34 mol_{CMA} min^{-1} g_{Pd}^{-1}, 0.24 mol_{CMA} min^{-1} g_{Pd}^{-1}, respectively, showing a strong size-dependent behavior which is in line with reported findings [13]. Besides, the specific rate of the 1.3 ±0.5 nm $Pd_{1.7}Co$/NC nanoparticles (0.5 mol_{CMA} min^{-1} g_{Pd}^{-1}) is more than three times and two times that of the 5% commercial Pd/C (0.15 mol_{CMA} min^{-1} g_{Pd}^{-1}) and $Pd_{1.7}Co$-T/NC (0.21 mol_{CMA} min^{-1} g_{Pd}^{-1}), respectively, benefiting from bimetallic synergies [46,47]. Hydrocinnamaldehyde (HCMA) selectivity over the 1.3 ± 0.5 nm $Pd_{1.7}Co$/NC nanoparticles (89 ±1%) is also found much higher than that of the 5% commercial Pd/C catalyst (71 ±2%). Catalytic stability test was conducted by recycling the postreaction 1.3 ±0.5 nm $Pd_{1.7}Co$/NC nanoparticles and 5% commercial Pd/C catalysts. As displayed in Figure S20, the hydrocinnamaldehyde selectivity over the 5% commercial Pd/ C catalysts drops from 72% to 63% in the second run and become stable around 64% in the following three runs. By contrast, our 1.3 ± 0.5 nm $Pd_{1.7}Co$/NC catalysts show excellent catalytic stability. As shown in Fig. 6d, after five cycles, the cinnamaldehyde conversion (95%) and hydrocinnamaldehyde selectivity (89%) over the 1.3 ±0.5 nm $Pd_{1.7}Co$/NC nanoparticles maintained well, demonstrating excellent catalytic stability of it. These results showed great potentials of our ligand-free and ultrasmall $Pd_{1.7}Co$/NC nanoparticles for practical applications.

3. Conclusion

To summarize, we report a self-limiting technique to prepare ultrasmall Pd-containing nanoalloys. The method is specifically useful to alloy base metals to noble metals such as Pd showing strong hydrogen spillover. The (co)reduction of the second base metal precursor (M = Co, Ni, and Zn) even under the thermodynamic reduction temperature of base metals was demonstrated, for the first time. The formation of bimetallic surfaces could turn down the further reduction of base metals that self-limits the overgrowth of bimetallic nanocatalysts. The surface alloys of Pd and other base metals changed the surface electronic state of Pd that improved the MOR catalytic activity and decreased the accumulation of carbonaceous residues. The high surfaceto-volume ratio of ultrasmall $Pd_{1.7}Co$ nanoalloys also endows them with great reactivity for selective hydrogenation of cinnamaldehyde. Our synthetic protocol is expected to provide a new guideline for preparation of highly efficient ultrasmall nanoalloys toward a variety of catalytic applications.

Author contributions

B. Liu and J. He conceived the project. M. Hu carried out the experiments with the help from L. Jin, Y. Zhu, L. Zhang, X. Lu, P. Kerns, X. Su, and S. Cao. P. Gao and S. Suib helped on surface characterizations of catalysts. All authors discussed the results and co-wrote the paper.

Declaration of Competing Interest

The authors declare no conflict of interest.

Acknowledgements

JH is grateful for financial support from the National Science Foundation (CBET-1705566) and the startup fund from the University of Connecticut. SLS acknowledges the support of the National Science Foundation under award 1803343 of the CBET Division. The SEM/TEM studies were performed using the facilities in the UConn/Thermo Fisher Scientific Center for Advanced Microscopy and Materials Analysis (CAMMA).

Appendix A. Supplementary data

Supplementary material related to this article can be found, in the online version, at doi:https://doi.org/10.1016/j.apcatb.2019.118553.

References

[1] S. Zhang, X. Zhang, G. Jiang, H. Zhu, S. Guo, D. Su, G. Lu, S. Sun, J. Am. Chem. Soc. 136 (2014) 7734–7739.
[2] J. Mao, W. Chen, W. Sun, Z. Chen, J. Pei, D. He, C. Lv, D. Wang, Y. Li, Angew. Chem. Int. Ed. 56 (2017) 11971–11975.
[3] S.J. Freakley, Q. He, J.H. Harrhy, L. Lu, D.A. Crole, D.J. Morgan, E.N. Ntainjua, J.K. Edwards, A.F. Carley, A.Y. Borisevich, C.J. Kiely, G.J. Hutchings, Science 351 (2016) 965–968.
[4] Q.-L. Zhu, J. Li, Q. Xu, J. Am. Chem. Soc. 135 (2013) 10210–10213.
[5] Y. Chen, Q.-L. Zhu, N. Tsumori, Q. Xu, J. Am. Chem. Soc. 137 (2015) 106–109.
[6] W. Chen, J. Kim, S. Sun, S. Chen, J. Phys. Chem. C. 112 (2008) 3891–3898.
[7] H. Liu, W. An, Y. Li, A.I. Frenkel, K. Sasaki, C. Koenigsmann, D. Su, R.M. Anderson, R.M. Crooks, R.R. Adzic, P. Liu, S.S. Wong, J. Am. Chem. Soc. 137 (2015) 12597–12609.
[8] G.S. Chaubey, C. Barcena, N. Poudyal, C. Rong, J. Gao, S. Sun, J.P. Liu, J. Am. Chem. Soc. 129 (2007) 7214–7215.
[9] D. Wang, Y. Li, Adv. Mater. 23 (2011) 1044–1060.
[10] K. Jiang, P. Wang, S. Guo, X. Zhang, X. Shen, G. Lu, D. Su, X. Huang, Angew. Chem. Int. Ed. 55 (2016) 9030–9035.
[11] R. Ferrando, J. Jellinek, R.L. Johnston, Chem. Rev. 108 (2008) 845–910.
[12] A. Wong, Q. Liu, S. Griffin, A. Nicholls, J.R. Regalbuto, Science 358 (2017) 1427–1430.
[13] L. Bai, X. Wang, Q. Chen, Y. Ye, H. Zheng, J. Guo, Y. Yin, C. Gao, Angew. Chem. Int. Ed. 55 (2016) 15656–15661.
[14] Y. Yao, Z. Huang, P. Xie, S.D. Lacey, R.J. Jacob, H. Xie, F. Chen, A. Nie, T. Pu, M. Rehwoldt, D. Yu, M.R. Zachariah, C. Wang, R. Shahbazian-Yassar, J. Li, L. Hu, Science 359 (2018) 1489–1494.
[15] H. Qian, M. Zhu, Z. Wu, R. Jin, Acc. Chem. Res. 45 (2012) 1470–1479.
[16] E.W. Zhao, R. Maligal-Ganesh, C. Xiao, T.-W. Goh, Z. Qi, Y. Pei, H.E. HagelinWeaver, W. Huang, C.R. Bowers, Angew. Chem. 129 (2017) 3983–3987.
[17] S. Wu, M. Li, Y. Sun, Angew. Chem. Int. Ed. 58 (2019) 8987–8995.
[18] Y. Hu, Y. Liu, Y. Sun, Adv. Funct. Mater. 25 (2015) 1638–1647.
[19] M.L. Personick, M.R. Langille, J. Zhang, C.A. Mirkin, Nano Lett. 11 (2011) 3394–3398.
[20] B. Liu, P. Wang, A. Lopes, L. Jin, W. Zhong, Y. Pei, S.L. Suib, J. He, ACS Catal. 7 (2017) 3483–3488.
[21] L. Jin, B. Liu, P. Wang, H. Yao, L.A. Achola, P. Kerns, A. Lopes, Y. Yang, J. Ho, A. Moewes, Y. Pei, J. He, Nanoscale 10 (2018) 14678–14686.

[22] B. Liu, H. Yao, W. Song, L. Jin, I.M. Mosa, J.F. Rusling, S.L. Suib, J. He, J. Am. Chem. Soc. 138 (2016) 4718–4721.
[23] K. Inoue, K. Yoshizuka, Y. Baba, Solvent Extr. Ion Exch. 8 (1990) 309–323.
[24] D. Parajuli, H. Kawakita, K. Inoue, M. Funaoka, Ind. Eng. Chem. Res. 45 (2006) 6405–6412.
[25] Y.F. Jia, B. Xiao, K.M. Thomas, Langmuir 18 (2002) 470–478.
[26] P.R. Zalupski, R. McDowell, G. Dutech, Solvent Extr. Ion Exch. 32 (2014) 737–748.
[27] G.X. Pei, X.Y. Liu, X. Yang, L. Zhang, A. Wang, L. Li, H. Wang, X. Wang, T. Zhang, ACS Catal. 7 (2017) 1491–1500.
[28] G. Kyriakou, M.B. Boucher, A.D. Jewell, E.A. Lewis, T.J. Lawton, A.E. Baber, H.L. Tierney, M. Flytzani-Stephanopoulos, E.C.H. Sykes, Science 335 (2012) 1209–1212.
[29] V. Mazumder, M. Chi, M.N. Mankin, Y. Liu, Ö. Metin, D. Sun, K.L. More, S. Sun, Nano Lett. 12 (2012) 1102–1106.
[30] A.-L. Wang, X.-J. He, X.-F. Lu, H. Xu, Y.-X. Tong, G.-R. Li, Angew. Chem. Int. Ed. 54 (2015) 3669–3673.
[31] D.A. Slanac, W.G. Hardin, K.P. Johnston, K.J. Stevenson, J. Am. Chem. Soc. 134 (2012) 9812–9819.
[32] M. Rezaei, S.H. Tabaian, D.F. Haghshenas, J. Mater. Chem. A Mater. Energy Sustain. 2 (2014) 4588–4597.
[33] G. García, M.T.M. Koper, Phys. Chem. Chem. Phys. 10 (2008) 3802–3811.
[34] Q. Jin, Y. He, M. Miao, C. Guan, Y. Du, J. Feng, D. Li, Appl. Catal. A Gen. 500 (2015) 3–11.
[35] C. Li, B. Jiang, N. Miyamoto, J.H. Kim, V. Malgras, Y. Yamauchi, J. Am. Chem. Soc. 137 (2015) 11558–11561.
[36] L. Wang, Y. Nemoto, Y. Yamauchi, J. Am. Chem. Soc. 133 (2011) 9674–9677.
[37] Q. Feng, S. Zhao, D. He, S. Tian, L. Gu, X. Wen, C. Chen, Q. Peng, D. Wang, Y. Li, J. Am. Chem. Soc. 140 (2018) 2773–2776.
[38] S. Guo, S. Zhang, X. Sun, S. Sun, J. Am. Chem. Soc. 133 (2011) 15354–15357.
[39] Y. Yang, L. Jin, B. Liu, P. Kerns, J. He, Electrochim. Acta 269 (2018) 441–451.
[40] L. Zhao, X.-L. Sui, Q.-Y. Zhou, J.-Z. Li, J.-J. Zhang, G.-S. Huang, Z.-B. Wang, J. Mater. Chem. A Mater. Energy Sustain. 6 (2018) 6212–6219.
[41] Z. Cui, M. Yang, F.J. DiSalvo, ACS Nano 8 (2014) 6106–6113.
[42] L. Zhao, X.-L. Sui, J.-Z. Li, J.-J. Zhang, L.-M. Zhang, G.-S. Huang, Z.-B. Wang, Appl. Catal. B 231 (2018) 224–233.
[43] J. Fan, S. Yu, K. Qi, C. Liu, L. Zhang, H. Zhang, X. Cui, W. Zheng, J. Mater. Chem. A Mater. Energy Sustain. 6 (2018) 8531–8536.
[44] Z. Yin, M. Chi, Q. Zhu, D. Ma, J. Sun, X. Bao, J. Mater. Chem. A Mater. Energy Sustain. 1 (2013) 9157–9163.
[45] L. Zhao, X.-L. Sui, J.-L. Li, J.-J. Zhang, L.-M. Zhang, Z.-B. Wang, ACS Appl. Mater. Interfaces 8 (2016) 16026–16034.
[46] X. Yang, D. Chen, S. Liao, H. Song, Y. Li, Z. Fu, Y. Su, J. Catal. 291 (2012) 36–43.
[47] S. Zafeiratos, S. Piccinin, D. Teschner, Catal. Sci. Technol. 2 (2012) 1787–1801.